Article published online: 2023-05-04

98

Organic Materials T. Mohammadi Hafshejani et al. Short Review

Chemical and Topological Control of Surfaces Using Functional Parylene Coatings

Tahereh Mohammadi Hafshejani[a]
Xiaoyang Zhong[b]
John Kim[b]
Bahar Dadfar[a]
Joerg Lahann* [a,b]

[a] Karlsruhe Institute of Technology (KIT), Institute of Functional Interfaces (IFG), Hermann-von-Helmholtz-Platz 1, 76344 Eggenstein-Leopoldshafen, Germany

[b] University of Michigan, Biointerfaces Institute, Ann Arbor, MI 48109, USA

* lahann@umich.edu

Unlimited Potential!

Abstract Chemical vapor deposition (CVD) polymerization is a prevalent technique for fabricating conformal, defect-free, and systematically adjustable organic thin films. CVD is particularly beneficial for barrier coatings due to its ability to eliminate solvent-related environmental, health, and safety risk factors and provide a wide spectrum of post-polymerization modification strategies. This review discusses poly-*p*-xylylene and its functional derivatives. CVD polymerization of [2.2]paracyclophane precursors has undergone a recent renaissance due to advancements in chemical and morphological surface manipulation. This review summarizes emerging trends based on the following outline:
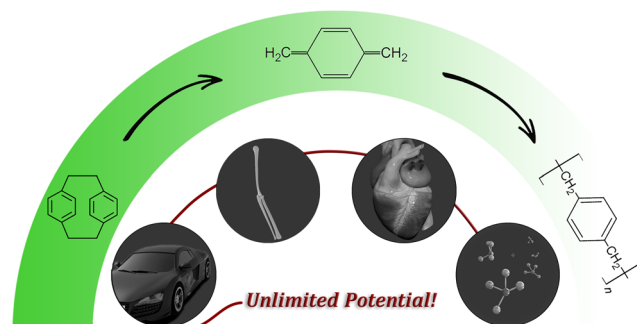
1 Introduction

Polymer coatings have impacted nearly every part of modern life due to their unique physicochemical qualities, including low density, restricted permeability, and resistance to degradation, which are largely the result of a diverse polymer chemistry.[1,2] Thin-film coatings of functional polymers, typically no thicker than 800 nm, have been developed to take advantage of polymers' extensive organic functions without compromising desirable bulk qualities (such as mechanical strength) of the underlying substrate.[1,3] Functional polymer coatings have been widely employed to define the surface properties of a variety of devices, thereby transforming research fields from energy and sustainability to medical devices. Despite the fact that solution-based techniques, such as layer-by-layer assembly,[4] inkjet printing,[5] and spin-dip coating,[6] continue to be important methods for forming polymer coatings in biological applications, vapor-deposited coatings have emerged as a promising alternative.

Chemical vapor deposition (CVD) is a chemical process involving the reaction of volatile precursors in the gas phase to produce a solid product that deposits on surfaces.[7] This method is commonly employed in the semiconductor industry to manufacture dense inorganic films.[8] Related to polymer thin films, precursors can adsorb to the surface first followed by a substrate-supported polymerization.[9,10] CVD processes tend to operate under low-pressure conditions because of the need to vaporize liquid (or solid) precursors and to avoid interactions of the precursors in the gas phase prior to deposition onto the substrate.[9] CVD polymer coatings have been successfully adopted in various applications during the last few decades, necessitating a systematic review. The purpose of this paper is to present a conceptual overview of recent advances in the control of surface properties through the fabrication of diverse poly-*p*-xylylene (PPX) structures employing CVD polymerization.

2 CVD Polymerization as a Sustainable Coating Technology

Numerous conventional chemical procedures include substantial quantities of poisonous and volatile organic solvents.[11] One of the primary goals of green chemistry is the replacement of such a harmful reaction solvent.[12] With increasing worldwide environmental consciousness, the design of solvent-free ("green") procedures has attracted re-

99

Organic Materials   T. Mohammadi Hafshejani et al.   THIEME OPEN ACCESS   **Short Review**

Biosketches

Tahereh Mohammadi Hafshejani received her Ph.D. degree in 2021 from Karlsruhe Institute of Technology (KIT), Germany, under the supervision of Dr. Peter Thissen. Her doctoral research centered on atomic-scale investigation of strain effect on surface properties of silicon and mineral materials. Currently, she is a postdoctoral researcher in the research team of Prof. Joerg Lahann at KIT. Her current research involves CVD surface modification focusing on polypeptides and conductive polymers.

Xiaoyang Zhong received her B.S. in macromolecular science and engineering from the East China University of Science and Technology. She received her M.S.E in materials science and engineering and is currently pursuing her Ph.D. in materials science and engineering from the University of Michigan. Her research focuses on the mechanism of area-selectivity of chemical vapor deposition polymerization.

John Kim studied materials science and engineering and received B.S. at Sungkyunkwan University in Republic of Korea. He is currently pursuing his Ph.D. in materials science and engineering at University of Michigan. His research focuses on the fabrication of functional nanofibers templated by liquid crystalline film using chemical vapor deposition.

Bahar Dadfar received her B.S. and M.S. in chemical engineering from Shiraz University (Iran) and Isfahan University (Iran), respectively. Currently she is pursuing a Ph.D. in chemical engineering at the Karlsruhe Institute of Technology (KIT) and her research focuses on screening various levels of protein–protein interactions using deep-learning approaches.
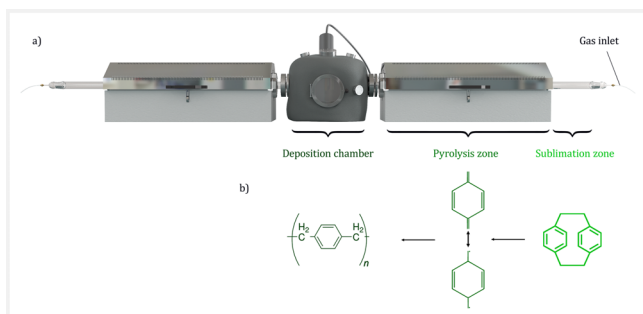
Prof. Lahann joined the University of Michigan in 2003 and has been the founding director of the University of Michigan Biointerfaces Institute since 2012. The Biointerfaces Institute is located on 56,000 sq ft of research space in the North Campus Research Complex and is the home to 33 research groups and about 400 researchers. Prof. Lahann is a co-author of more than 315 publications and has contributed to more than 50 patents and patent applications. He has been selected by Technology Review as one of the top 100 young investigators and the recipient of the 2007 Nanoscale Science and Engineering Award, an NSF-CAREER award. He is a member of the National Academy of Inventors and a fellow of the American Association of the Advancement of the Sciences (AAAS) and the American Institute of Medical and Biological Engineering.

searchers' attention. Many processes using solid-state or solvent-free conditions have been prioritized due to reduced pollution and expense.[13] These reactions make procedural work much simpler and more efficient; hence, they have gained vital importance and popularity in a short period of time.[13,14] Following the mindset of sustainability, future polymer coatings necessitate a strong focus on greener approaches. The concept of using more sustainable solvents, such as water, polyethylene glycol, molten organic salts, and supercritical CO_2, to replace conventional organic solvents is thus gaining support.[15] Alternatively, a wide variety of reactions have been advanced to occur in the solid form entirely without the need for a solvent. CVD polymerization as an entirely solvent-free procedure fits into this classification and thus broadens the applications for polymeric surface modification.[16] Removing the requirement for solvents has also important performance implications, because it eliminates the possibility of bridging, meniscus and swelling effects. Moreover, curing or thermal treatments are unnecessary and leaching of contaminants is generally not a concern typically resulting in superior biocompatibility.[16,17] In addition to its advantages for highly controllable film production, the fabrication of solvent-free polymeric layers using the CVD process may have a significant technological impact that appears to favorably align with current green and sustainable trends in surface engineering.

3 CVD Instrumentation

CVD systems typically have four parts (Figure 1a): a gas inlet, where vaporized precursors (like monomers) are delivered into the deposition chamber; sublimation and pyrolysis zones, where the precursor is converted into reactive monomers; and a deposition chamber, where the precursors are chemically activated to enable subsequent polymerization reactions on or near the substrate surface.[2,18] The primary classification of CVD methods is based on either their reaction mechanisms or their energy sources [for example, plas-

ma-enhanced CVD (PECVD)].[19] Functional polymer thin films can be created using CVD procedures via chain-growth or step-growth polymerization mechanisms. The chain-growth mechanism is used in methods such as initiated CVD (iCVD)[7,20] and PECVD,[21] whereas the step-growth mechanism allows for the reaction to occur between any two nearby molecules with the right moieties. The latter is frequently observed in PPX polymers[22] and oxidative CVD (oCVD).[23]

The processes described above, including iCVD, "parylene-type" CVD polymerization, PECVD, and oCVD, are among the methods that are utilized the most frequently in the production of functional polymer thin films for use in biological applications. In interface engineering for biological applications, CVD polymerization of [2.2]paracyclophanes (PCPs) is one of the most prevalent techniques.

4 Poly-*p*-xylylene Coatings: Background of Polymerization Process and Functionalized Films

In the ground-breaking research carried out by Gorham, PCP vapor was subjected to thermal cracking (Figure 1b).[24,25] In 1947, Szwarc first described the production of PPX using vacuum polymerization.[26] Building upon these earlier efforts, the Gorham approach for CVD polymerization of PCP broadened its practical applicability.[25] The PCP precursor is converted into reactive monomers using sublimation and vacuum pyrolysis at temperatures exceeding 600 °C (Figure 1b).[27] William Gorham demonstrated that PCP can be quantitatively transformed into monomers at 600 °C.

Soon after the discovery of PPX, scientists demonstrated that functionalized PPX films can further enhance coating performance.[28] The chemical structures and trade names of most common derivatives are illustrated in Figure 2. PPX-C is the most widely used PPX derivative because of its strong

Figure 1 a) A side-view schematic of a two-source CVD system. CVD reactor typically consists of 4 main parts: gas inlet, sublimation zone, pyrolysis zone and deposition chamber. b) Polymerization process of [2.2]paracyclophane to PPX under the conditions given in a CVD system.
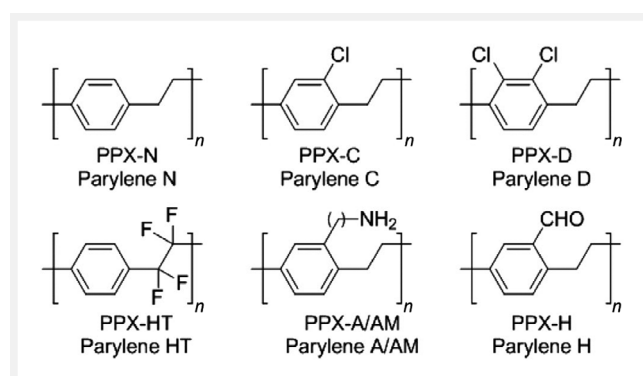

Figure 2 Chemical structure of the most common commercial PPX or parylenes (trend name). Adapted from Ref. 24 published under a creative commons license (CC BY).

dielectric and moisture barrier properties.[24] The demand for functional polymer coatings is significant, particularly in biomaterials research. The surface functionality of PPX can be utilized to derivatize the coating after deposition, resulting in the formation of intriguing biological interfaces.[28] By altering surface properties based on polymerization precursors, this could open up new paths for biomaterials engineering. To improve implant biocompatibility, reactive PPXs could be functionalized with biomolecules, such as proteins or biopolymers.[28,29]

For this approach, chemical groups that can serve as chemical anchors and to which biomolecules can form covalent bonds are necessary. Employing functionalized PPX, for instance, has enabled the surface modification of metallic stents with a range of reactive coatings, such as poly(*p*-xylene-2,3-dicarboxylic acid anhydride), which was essential for the covalent immobilization of r-hirudin.[30] In a separate investigation, scientists discovered that poly(hydroxymethyl-*p*-xylylene-co-*p*-xylylene)-coated stents exhibit excellent mechanical stability, outstanding biocompatibility, and low in vitro and in vivo cytotoxicity.[31] The precursor is functionalized prior to polymerization, resulting in reactive CVD coatings. It is challenging to produce precursors that can be sublimed, are thermally stable at pyrolysis temperatures, and capable of forming *p*-quinodimethane (i.e., PX) as the reactive monomers of CVD polymerization.[24] Since the establishment of the Gorham process, many projects have used functionalized PCP with success.[32]

As precursor, difunctionalized PCP and monofunctionalized PCP are the two most common ways to obtain PPX derivatives.[24] By adding bulky groups to the benzyl ring, it was possible to produce solvent-soluble polymers.[33] Due to their solubility, these polymers may be studied using traditional techniques such as gel permeation chromatography and nuclear magnetic resonance (NMR) spectroscopy. Introduction of n-alkyl chains at the benzylic ring also resulted in polymers where glass transition temperature, decomposition temperature, and Young's modulus decreased with increasing alkyl chain length. In addition to solubility, functionalization can affect a large number of other characteristics. Siloxane substituents, for instance, produced an amorphous, colorless polymer with a glass transition temperature of $-10\,°C$ and a 5% decomposition temperature of $442\,°C$.[33] This polymer possessed superior mechanical properties compared to unsubstituted PPX, with a Young's modulus of 0.02 GPa and an average elongation at break of 470%. Additionally, the siloxane groups altered the wetting behavior. As previously demonstrated for the siloxane-modified PPX, the elongation at break (maximum value of 380%) was also enhanced compared to commercial PPX. Using a monosubstituted PCP, several functionalized PPX surfaces were prepared.[24] CVD polymerization of these precursors led to the formation of a copolymer composed of PX and the substituted PX building blocks. Due to the dissimilar vapor pressures of the quinodimethanes, it is difficult to produce copolymers with equal amounts of each monomer moiety.[34] Lahann and colleagues employed monosubstituted PCP as the starting material for a variety of functionalized coatings.[28,35] They used their coatings primarily to immobilize biomolecules such as proteins and cells. Additionally, functionalized PPX was employed to immobilize proteins using site-specific and nonspecific coupling strategies. Maleimide- and *N*-hydroxy-succinimide-substituted PPX copolymer was created as a result.[36] The simultaneous pyrolysis of two distinct precursors in distinct sublimation and pyrolysis zones permitted the formation of copolymers with three building units.[37]

5 Main Applications of Poly-*p*-xylylenes

The application fields are dominated by two categories: electronics and medicine.[38] In both domains, polymers perform coating and protection functions. PPX is a typical protective coating used in the sectors of electronics, aerospace, and medicine.[39,40] Up to a given thickness, the resulting film is chemically resistant, thin, conformal, and free of pinholes. The coatings confer a multitude of properties simultaneously, including enhanced lubricity, electrical insulation, chemical and moisture isolation, and mechanical protection. Dust and soil are repelled by the low adhesion to the surface. The surface of PPX coatings can be altered using a specialized plasma coating. Thus, an interlayer is placed to provide excellent adhesion to both the substrate and the subsequent primer. Following this procedure, the hydrophobic PPX polymer can once again be painted using solvent-borne or waterborne spray primers.[39]

PPX can be applied to change biological surface properties. Diverse chemical anchor groups produce a coating platform that is flexible.[28,41] The most prevalent use of PPXs in the medical industry is as protective coatings for a vast array of devices.[28] Surface engineering for microfluidic devices is made possible by the CVD polymerization's ability to synthesize a variety of functional groups.[42] Insulin has been immobilized on surfaces with CVD coatings to facilitate in vitro cell adhesion and proliferation. As functionalization anchors, amino groups that dangle from copolymers with amino-*p*-xylylene and PX moieties can act as amino groups. These amino groups are capable of immobilizing thrombin inhibitors such as r-hirudin. The functionalization is useful for devices that come into contact with native blood.[43] Inhibitor of thrombin r-hirudin has been introduced to the pharmaceutical release system.[44] Frequently, the capacity of biosensing and bio-MEMS to accomplish their functions depends on their surface attributes (such as wetting characteristics, binding to biomolecules, etc.).[45] Therefore, interface engineering is crucial. Consequently, biosensing apparatus and microfluidic devices usually require functional

polymer coatings on the device surface for their construction and/or performance enhancement.[2,28] As a result of its conformability, CVD processes are widely employed as coating techniques. During manufacture, surface micro- and nanostructures are routinely added to biosensors and bio-MEMS devices to boost their surface-to-volume ratio, enabling sensitive detection and precise manipulation at the biointerface.[46] Coatings made of PPX have been utilized to increase the sensitivity of fluorescence imaging as well as to create sensor arrays that are employed in label-free molecular identification.[37] CVD coatings are therefore new substrates for studying biomolecule–surface interactions when quantitative and spatial information is sought.[28,37] In addition, a wide variety of biomolecules have been immobilized using functionalized PPX containing aldehydes,[47] amines,[48] anhydrides,[49] or active esters.[41,50] In biosensing, fluorescence imaging is frequently used to visualize cells or other living things in situ with high spatial resolution. PPX coatings have been used to overcome the signal-to-noise ratio issues of certain biological systems.[51] Additionally, the varied functional moieties of CVD polymer thin films enabled facile biofunctionalization for precise interaction with target molecules. These imaging substrates with CVD alterations revealed ultrasensitive in situ detection of target biomolecules.[2]

6 Area-Selective CVD Polymerization

In order to generate arrays of nanoscale features at high densities, numerous surface preparation and treatment techniques involving multiple steps are developed. Microcontact printing (μCP) is one of the most widely used patterning techniques, employing patterned elastomers to imprint reactive chemicals on polymer-modified substrates.[52] Applying a photomask to the vapor deposition of polymer films on perfect substrates is an additional frequent patterning technique. These two methods are based on photo- or soft-lithographic processes.[52,53] These techniques are restricted to traditional two-dimensional surfaces due to the limitations of photomasks and elastomeric stamps.[54]

Combining nanolithography,[56] e-beam lithography,[57] and two-photon laser with vapor-deposited polymer films enables the creation of micro- or nanostructures on surfaces with complex geometries. This is due to the fact that vapor-deposited polymer films offer conformal coverage, adjustable ultra-thin (20 nm) thickness, pinhole-free construction, and programmable topology and chemistry.[58] In addition to being used in the patterning of three-dimensional structures, they are also widely employed in electronics as a tunable organic dielectric layer and in biology for localized surface modification.[59] Nevertheless, these methods are costly, time-consuming, chemically demanding on the environment, wasteful, and toxic. Thus, area selective deposition (ASD) is a more suitable technique for achieving this objec-

tive.[60,61] In general, ASD results in conformal deposition of polymer layers on desired 'favorable' substrates/regions and no or minimal deposition in intended 'unfavorable' regions.[61]

Since the beginning of the 20th century, ASD has been used in CVD polymerization. Gladfelter determined the selectivity of area-selective CVD using Equation 1.[62]

$$S = \frac{\theta_1 - \theta_2}{\theta_1 + \theta_2} \qquad (1)$$

Instead of measuring the quantity of nuclei on the surface, Gladfelter compared the preference of deposition during initial deposition using the easily measured nucleus coverage. The overall selectivity, S, can be determined by comparing the difference between the nuclei coverage on surface 1, θ_1, and surface 2, θ_2. Vaeth and Jensen discovered that iron and its salt had significant implications for preventing poly(p-phenylene vinylene) formation on the substrate surface during CVD by limiting the nucleation and propagation steps.[63]

The polymerization inhibition effect was extended to transition metals, transition metal salts, and organo-transition metal complexes.[64] As the most prevalent PPX, PPX-N and PPX-C also exhibit ASD. Suh et al. produced nanoscale structures by combining CP and selectively deposited CVD polymerization.[55] Their methods (Figure 3a) include creat-
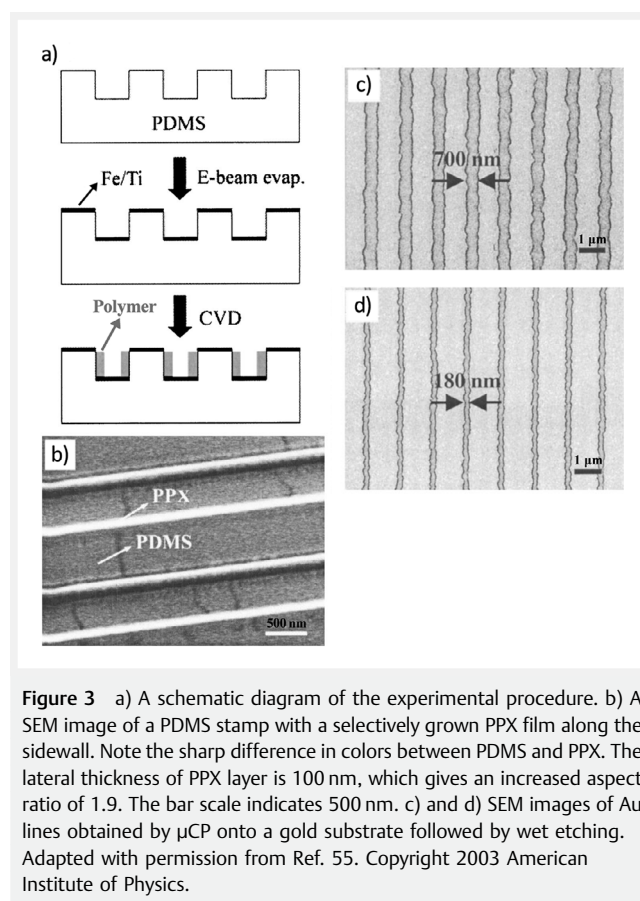
Figure 3 a) A schematic diagram of the experimental procedure. b) A SEM image of a PDMS stamp with a selectively grown PPX film along the sidewall. Note the sharp difference in colors between PDMS and PPX. The lateral thickness of PPX layer is 100 nm, which gives an increased aspect ratio of 1.9. The bar scale indicates 500 nm. c) and d) SEM images of Au lines obtained by μCP onto a gold substrate followed by wet etching. Adapted with permission from Ref. 55. Copyright 2003 American Institute of Physics.

ing PDMS stamps with photolithographic patterns, coating inhibitor layers with titanium and iron films solely on flat top and bottom surfaces using e-beam evaporation, and applying PPX via CVD polymerization. PPX deposited only on the walls of PDMS stamps due to iron's inhibiting effect. Further scanning electron microscopy (SEM; Figure 3b) measurements were used to identify the structures with a high aspect ratio. Using μCP, the technical utility of the modified stamp was further evaluated; Figure 3c,d demonstrates successful pattern transfer.

As shown in Figure 4,[65] Chen et al. examined the specific inhibition of CVD polymerization by a variety of metals using a systematic approach. They applied selective inhibition to reactive polymer coatings such as functionalized PPX. No area-selective property was identified on transition metals

for oxygen- or nitrogen-containing substituted PPX. This suggested that the metal and the heteroatoms interact preferentially. In addition, not all metals exhibited selectivity for the same polymer. Certain substrates, such as iron, copper, silver, platinum, and their salts, are more likely to inhibit CVD polymerization.[65] Using density functional theory calculations, Vitos[66] and his colleagues confirmed that substances with high melting temperatures typically have high bond strengths; for example, the surface energy of tungsten is anticipated to be more than that of its neighbor molybdenum and substantially greater than those of noble metals. In addition, high-index facets often have a greater surface energy than low-index facets due to a higher density of low-coordinated surface atoms; for instance, the surface energy of Rh{830} is more than that of Rh{100}.[67] In fcc, bcc, and
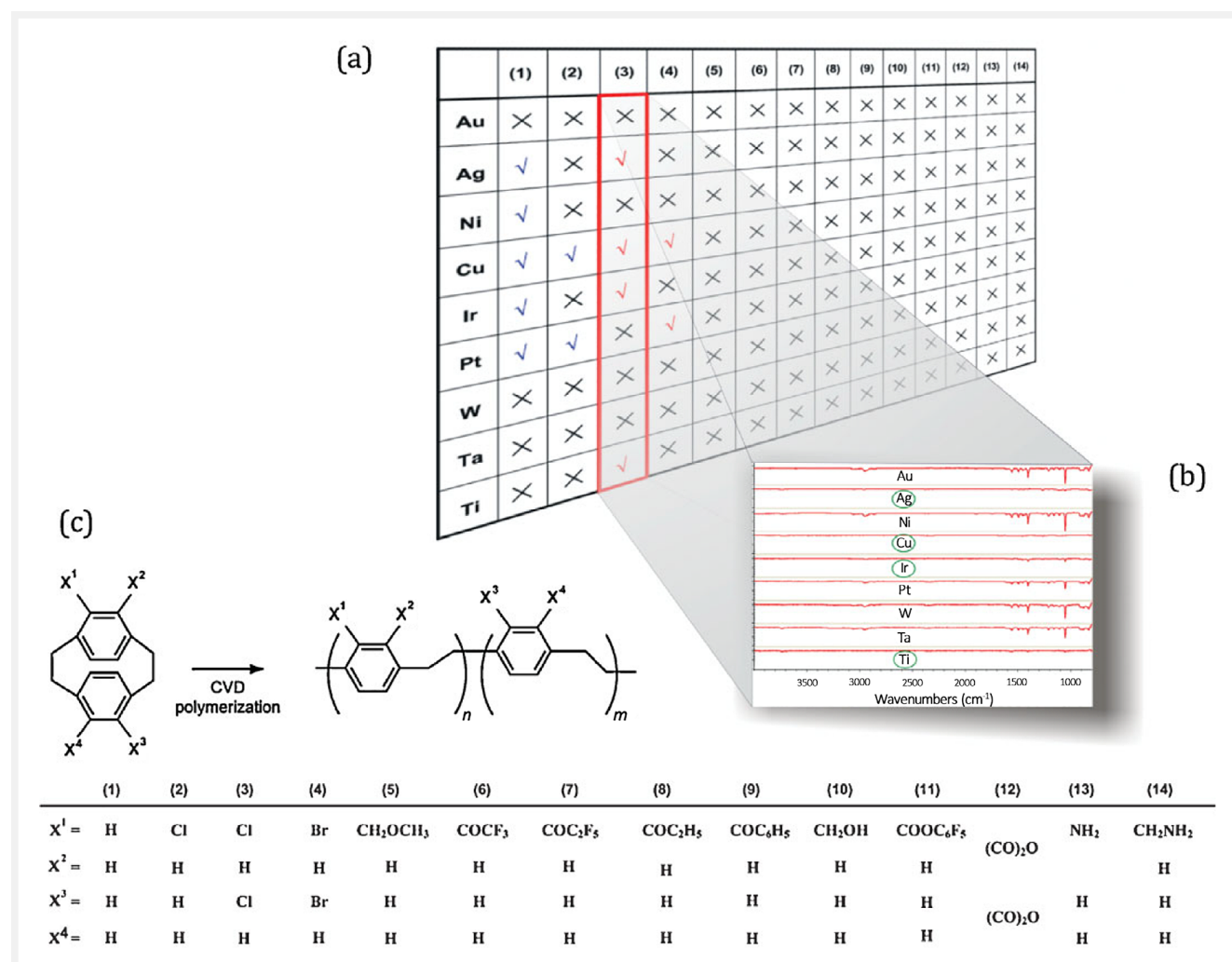
Figure 4 (a) Area selectivity on nine different metal surfaces (Au, Ag, Ni, Cu, Ir, Pt, W, Ta, and Ti) for poly-*p*-xylylenes deposited via CVD polymerization. (b) Typical spectra for poly(dichloro-*p*-xylylene) (3) on Au, Ag, Ni, Cu, Ir, Pt, W, Ta, and Ti. The spectra are dominated by characteristic C–Cl stretches at 1030–1100 cm^{-1}, which were present on Au, Ni, Pt, W, and Ta surfaces, but not on Ag, Cu, Ir, or Ti surfaces. (c) Schematic illustration shows the CVD polymerization process of PCP that yields nonreactive (1–4) as well as reactive (5–14) poly-*p*-xylylenes. Adapted with permission from Ref. 65. Copyright 2008 John Wiley and Sons.

hcp materials, the {111}, {110}, and {0001} planes have the highest atomic density per unit area, respectively.[68] According to the classic broken bond model, the minimizing of broken bonds in these surfaces leads to the lowest surface energy values.[68] Chen et al. reported that the growth of poly [4-vinyl-*p*-xylylene-co-*p*-xylylene] was selectively inhibited on titanium and confirmed its reactivity for spatially controlled cross-metathesis reactions.[65] With its functional groups, this selectively deposited reactive coating may offer an exceedingly straightforward technique for designing micro- and nano-structured biointerfaces.

Physisorption of the monomer on the surface and subsequent chemisorption are two steps in the multistep process that is described as the growth mechanism in CVD. The chemisorption step is analogous to a propagation reaction between the monomer and a radical chain end, and each chemisorption produces a new chemisorption site.[69] The plausible explanation is that the initiation reaction happened when two or more monomer molecules combined to form a biradical oligomer following the adsorption of monomers on the substrate. The propagation process began when a monomer molecule reached one of the free-radical polymer chain ends.[70] Fortin and Lu developed a kinetic model in which the rate-limiting phase of polymer synthesis was precursor adsorption on the surface.[69]

In the Fortin model, the sticking coefficient, which is determined by the energetics of the monomer–substrate interaction, is defined as the probability of a precursor species adsorbing or reacting each time it strikes the surface, and is normally controlled by the substrate temperature. It is essential to remember that the sticking coefficient only applies to chemisorption processes. Each initial monomer that chemisorbs in the absence of sufficient coverage will result in a new radical chain termination (similar to nucleation in crystal formation). In Figure 5a, the experimental data indicate clearly that the sticking coefficient of PX reactive species is proportional to temperature; consequently, the deposition rate is likewise proportional to the deposition temperature.

As depicted in Figure 5b, the deposition rate of PPX generally increases as substrate temperature decreases. indicating that the adsorption is the rate-limiting step. Working pressure inside the CVD system is another crucial factor that influences the deposition rate, shown in Figure 5c, as it influences the concentration of gas-phase precursor species. In this case, the deposition rate increases as the operating pressure rises. Nowadays, it is of technological importance to scale down electronic devices, especially semiconductors and microchips, to get faster performance with smaller sizes, which fuels a need for complex three-dimensional structures and thin-film materials. ASD, as one of the technologically relevant bottom-up technologies, allows for synthesis of nanomaterials with well-defined shapes, sizes, and chemical compositions that are formed through the growth
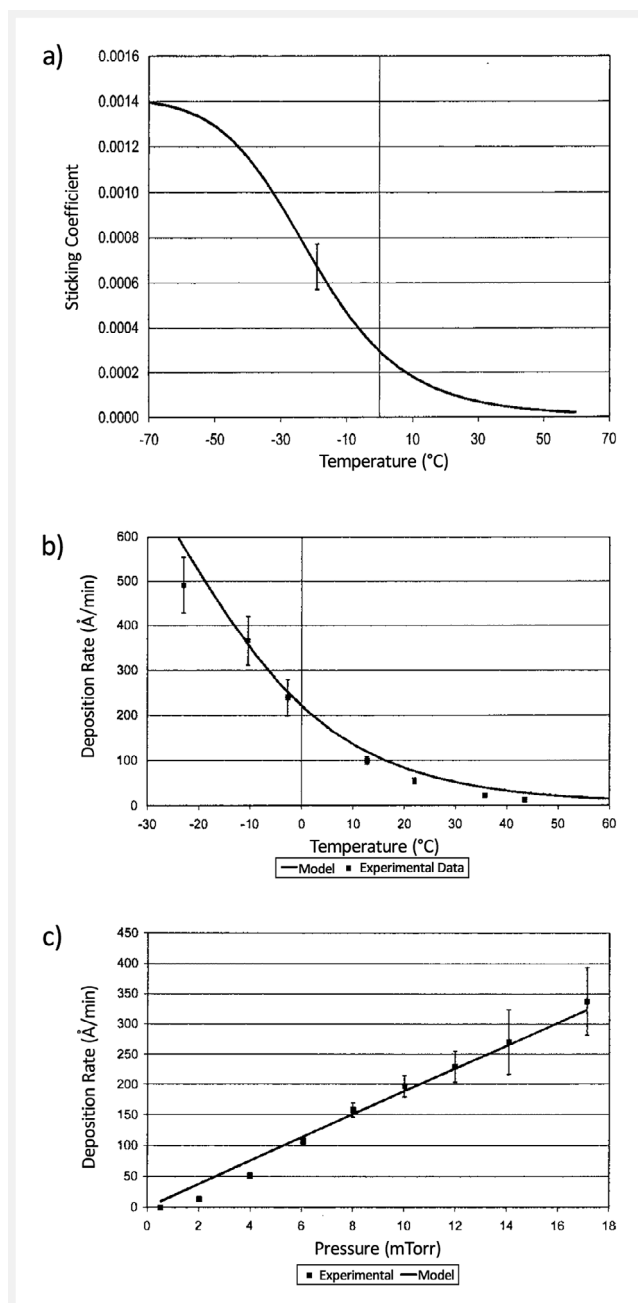
Figure 5 a) Sticking coefficient of PX reactive species as a function of temperature. b) Deposition rate as a function of temperature at pressure = 4.0 mTorr. c) Deposition rate as a function of pressure at temperature = 22 °C. Adapted with permission from Ref. 69. Copyright 2002 American Chemical Society.

and self-assembly of atoms and molecules as their building blocks.[71] Unlike atomic layer deposition, which requires removal of residual deposits to avoid the deposition on a nontarget area during ASD, CVD polymerization provides a new ASD strategy.[61] Moreover, recent kinetic studies suggest the

deposition conditions during CVD polymerizations, including temperature and pressure, are the main effect of deposition rate. Although the precise underlying mechanism of area-selectivity in CVD polymerization is yet to be understood, it is critical to investigate the relationship between area-selective CVD polymerization and deposition conditions.

7 Fabrication and Applications of Topological Structures

For many years, approaches for the fabrication of topological structures have been of interest as a progression beyond surface film coating. Numerous attempts have been made to leverage the unique properties that certain topologies, dimensions, and chemistries can provide, such as chirality, targeted drug delivery, and supramolecular assembly; however, the majority of techniques have limited access to offer tailoring the shape of a material with multiple functionalities. In this context, CVD polymerization offers distinct benefits for the fabrication of PPX structures with the appropriate forms and characteristics. In particular, adding a template for polymerization allows its shape and physicochemical properties to be transferred to the resultant structures.

Chen and colleagues employed ice particles as the template for CVD polymerization to produce porous PPX architectures in their research.[72] They sprayed water mist onto a superhydrophobic surface (modified silicon or glass) to generate water droplets with a high contact angle (static, advancing, and receding angles of 152.0° ± 0.9°, 154.1° ± 0.6°, and 150.2° ± 0.8°, respectively). The specimen was then vitrified by immersion in liquid nitrogen and placed on the CVD reaction chamber. Under the conditions of 100 mTorr and 4 °C, vaporized monomers of the PPX were deposited onto the sublimating ice particles. This diffusion-limited deposition/sublimation technique produced porous PPX particles with sizes constrained by the ice particle templates. By initiating sublimation at a specified time, the sizes of ice particles and consequent PPX particles may be regulated. They then adopted an ice-templated CVD system for applications in multifunctional, multicompartmental, and cell-laden scaffolds.[73] They also designed multicompartmental scaffolds by spatially assembling two ice templates with different geometries and microenvironments.

In a recent work by Tsotsalas and co-workers, crystal-controlled CVD polymerization using metal–organic frameworks (MOFs) as the template was used to create porous microparticles (Figure 6).[74] They used PPX and PPX-C for the deposition and HKUST-1 as a sacrificing MOF crystal. After CVD deposition, PPX@MOF composites were formed and then placed in a basic solution in order to remove the template and create monolithic PPX particles. To evaluate the depth of PPX precursors into the MOF templates, the PPX
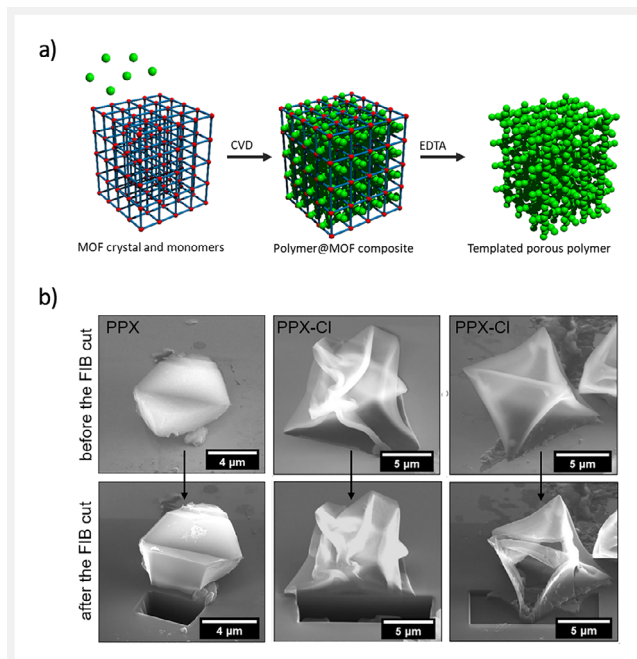
Figure 6   Top: Schematic illustration of the polymerization of PPX via cyclophane-based CVD polymerization using MOF crystals as a template. EDTA stands for ethylenediaminetetraacetic acid. Bottom: Crystal shape and cross-section of the PPX particles PPX and PPX-Cl before and after the FIB cuts. Reproduced with permission from Ref. 74. Copyright 2022 American Chemical Society.

particles were analyzed via focused ion beam SEM (FIB-SEM). Cross-sectional SEM images of PPX particles revealed a solid core, whereas PPX-C particles had a hollow interior (Figure 6b). The authors further utilized PPX and PPX-C porous particles as reversible ethanol gas adsorbent materials showing substantial uptake of the gas by ~ 320 ng/µg and ~ 40 ng/µg, respectively. The difference in uptake rate was attributed to the porous morphology of PPX particles which was able to host more ethanol vapors to the particles compared to the PPX-C that behaved similarly to the reference sensor. Compared to other precedent methods, such as free-radical polymerization,[75] electropolymerization,[76] and click reaction,[77] MOF-templated CVD allows for fabrication of nanoscale porous gas-hosting particles without yielding solvents, catalysts, and byproducts.

To further exploit the merits of templated micro- and nanoscale materials, it is important to modulate their chemical and structural features diversely. Topological architectures, in many cases, leverage their large surface-to-volume ratio or porous properties for specific applications. In this context, fibrillar structures are another class of materials that have attracted large interests for a variety of applications. Greiner and co-workers reported PPX microfibers templated by electrospun poly(L-lactide) (PLA) fiber.[78] The PPX-PLA core-shell fibers were annealed at 250 °C under

106

**Organic Materials**   T. Mohammadi Hafshejani et al.   THIEME OPEN ACCESS   **Short Review**

vacuum to degrade the PLA templates and obtain PPX hollow tubes. They also explored electrospun poly(vinyl alcohol)/bovine serum albumin (BSA) nanofibers for the application of release time control of BSA via coating nanometer-thick (40–300 nm) PPX coating on the composite fibers.[79] Demirel and co-workers have shown a template-free synthesis of submicron wires using oblique angle deposition.[80] They have outlined a template-free synthesis of submicron wires using oblique angle deposition.[80]

They have reported a template-free synthesis of submicron wires using oblique angle deposition.[80] There are two challenges to overcome to make fibrous structures without using template materials: 1) CVD tends to result in dense polymer films, which is not a desirable feature with respect to engineering fibers that are inherently porous, and 2) the flux of monomer deposition is non-directional. To resolve these issues, they customized CVD by adding a nozzle for the directional deposition and assembled two rotating motors with two axes that are vertical and planar to the substrate. They discovered that slanting the substrates away from the deposition axis offers porosity and leads to formation of sculptured thin films of PPX. From the oblique angle deposition, as represented in Figure 7A, a columnar morphology (aspect ratio of ~1 : 1000) that is tilted away from the surface normal was obtained on a substrate.

They were able to further modulate the structures by rotating the stage planarly to fabricate helical and chevron morphologies (Figure 7B,C). Templated CVD polymerization has demonstrated its potentials to make tailored structures of fibers owing to their excellent coverage on the solid-state materials and modular process parameters (e.g., pyrolysis temperature, stage temperature, and deposition rate of the

Figure 7   Cross-sectional SEM micrographs of columnar (A) columnar, (B) helical, (C) chevron and (D) planar PPX films. Planar PPX films do not possess nanostructured morphology. Scale bars for all micrographs are 20 µm. Reproduced with permission from Ref. 80. Copyright 2008 Elsevier.

PCP precursors). While solid templates enable straightforward deposition on the surfaces, using fluid templates offers more unique architectures due to their dynamic interplay with guest materials. Aizenberg and co-workers coprecipitated $BaCl_2$ and Na_2SiO_3 under constant flow of CO_2 to spontaneously form cylinder, petal, coral, or helical structures depending on the concentration of carbonate nucleation density and overall pH of the solution.[81] While chemical interaction plays key roles in templating, turbulent flow-induced molding was also demonstrated to engineer polymer into spherical, fibrous, or dendritic polymer particles.[82]

Anisotropic liquids, specifically liquid crystalline (LC) phases, are also an interesting option for templating material owing to their unique long-range order of alignment and elastic properties.[83] Kato and co-workers have used smectic LCs to make a hydrogen bond-assisted nanofiber network.[84] The alignment of nanofibers was in accordance with the local LC orientation and changed by slight tuning of the temperature. Akagi and co-workers templated polyacetylene nanofibers with a variety of LCs with catalysis into chiral nanofibers.[85] Integrating the advantages of CVD with LCs, LC-templated CVD polymerization resulted in the synthesis of end-attached nanofiber arrays supported by a solid surface.[86] A film of LC supported by a glass substrate was transferred to the CVD reaction chamber and pyrolyzed monomers diffused into the LC template to form nanofiber arrays (Figure 8D). After removing LC by rinsing with organic solvents, they noted that the alignment of nanofibers was in accordance with the molecular ordering of the LC template. For instance, nematic LC film with homeotropic (vertical) anchoring to the substrate formed straight nanofibers, while adopting cholesteric LC film-induced helical nanofibers. Optical characterization with crossed and transmission electron microscopy diffraction pattern revealed nematic-like ordering of polymer chains within the nanofibers (Figure 8F–I). Lahann and team further modulated the morphology of nanofibers into enantiomerically pure nanohelices using a precursor with chiral center.[87] Compared to conventional methods to fabricate chiral nanofibers (e.g., electrospinning[88] or molecular self-assembly[89]), LC-templated CVD decorated the surface with an ordered array of nanohelices in the achiral LC (Figure 9). They reported that the molecular chirality of chiral PCP was transferred to cause helicity in nanofibers and spiraling of nanofibers in a higher order of scale. Depending on the ratio of chiral (Figure 9B,C) and achiral precursors (Figure 9D), their copolymerization using CVD enabled the control over chirality of nanohelices. After dispersing nanohelices in methanol by bath sonication, circular dichroism (CD) spectroscopy revealed mirrored signals at 242 nm with characteristic Cotton effects indicating that molecular chirality being transferred to the nanohelices. In contrast, achiral nanofibers did not exhibit any conspicuous signals of CD spectrum. To further understand the role of the molecular chirality of PCP to its surrounding LC
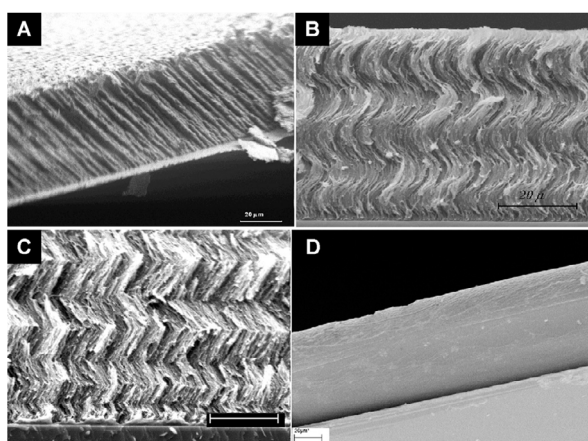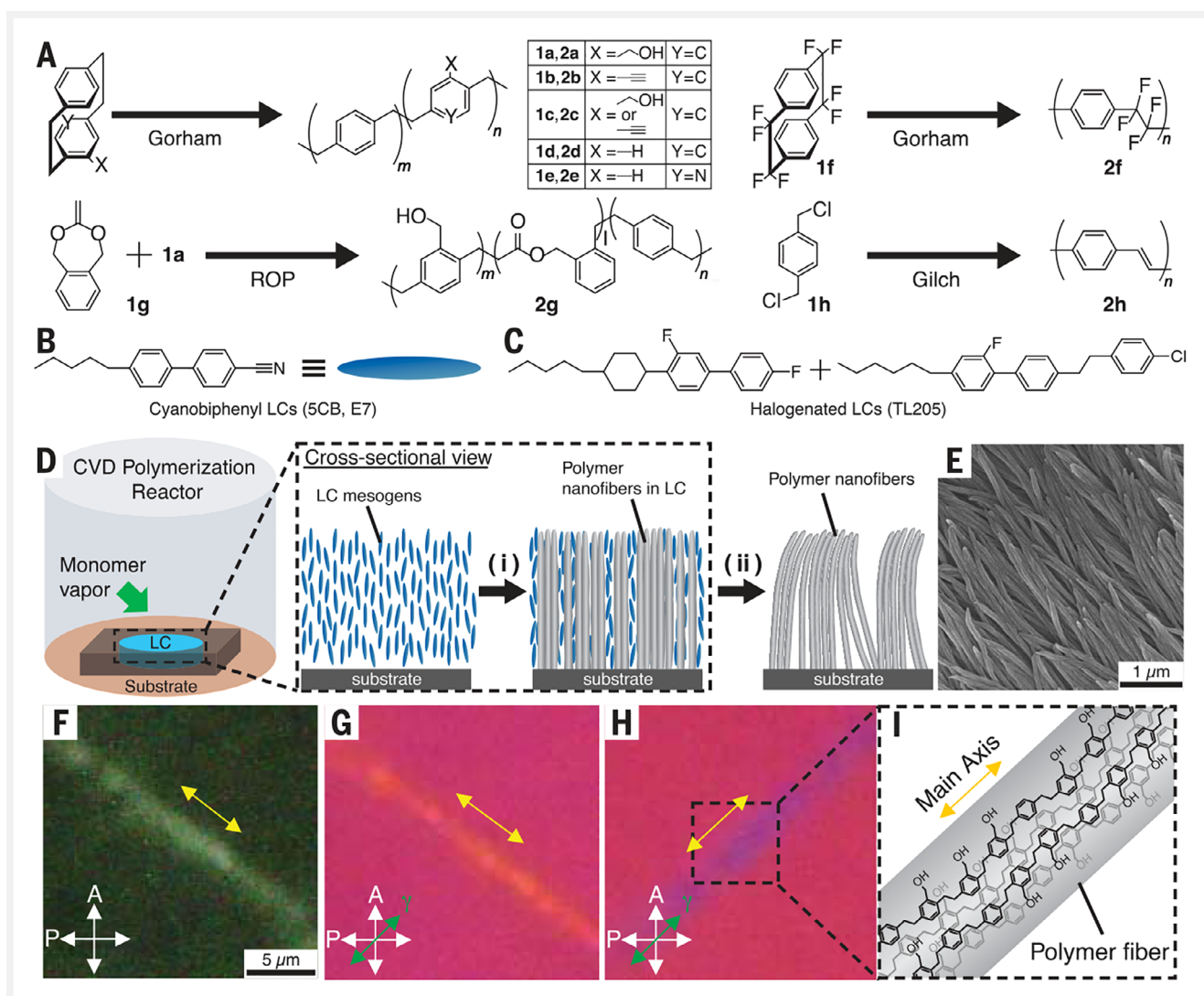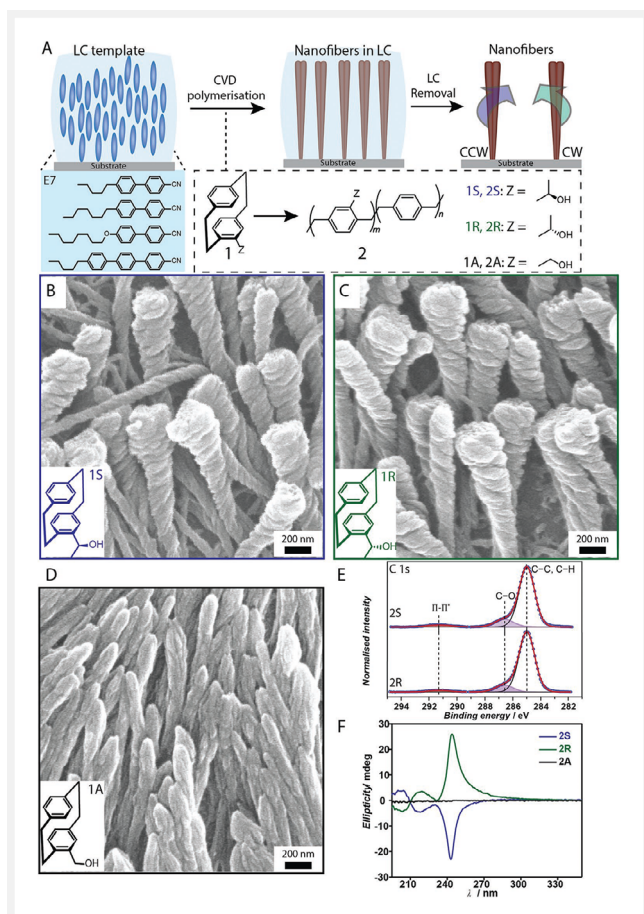
Figure 8   Templated synthesis of nanofiber arrays via CVD into anisotropic media. (A) CVD of 1a–h yields polymers 2a–h. (B, C) Representative chemical structures of cyanobiphenyl-based (5CB and E7) and halogenated (TL205) LCs. (D) Fabrication of polymer nanofibers via CVD into a LC phase aligned perpendicular to the substrate. (E) SEM images of nanofibers polymerized from 1a (10 mg) in 5CB. After the nanofiber synthesis, the LC template was removed. (F) Optical micrograph (crossed polars) of a nanofiber. Orientations of the analyzer (A) and polarizer (P) are shown in the double-arrow cross. (G, H) Micrographs (crossed polars) of the nanofiber with a quarter wave plate with its slow axis (γ, green double arrow) (G) perpendicular or (H) parallel to the fiber axis; lower order interference colors (yellow) indicate a decrease in retardance. (I) Analysis of interference colors of the nanofiber in (G) and (H) indicates orientation of the polymer chains aligned along the fiber axis. Adapted with permission from Ref. 86. Copyright 2018 The American Association for the Advancement of Science.

template, they replaced nematic LCs with cholesteric LCs to investigate competing chirality effects between the precursors and templates. When the chirality of the precursor and the LC template was identical, CVD polymerization resulted in supercoiled nanohelices while they obtained straight nanohelices with precursor and LC with countering chirality. This discovery has a couple of important implications: 1) understanding how the chirality is transferred across the multiple scales in artificial and natural systems and 2) a

new platform to fabricate nanohelices with control over the alignment and scales.

Advancing the fundamental understanding on nanofiber-templates, it is critical to explore how nanofibers share elastic strain with LC template under an electric field.[90] One of the interesting properties of LC is dielectric property, which causes changes in molecular orientation when an electric field is applied. From morphological modulation by inherent LC phases in their previous report, they demonstrated the synthesis of bent nanofiber arrays that exhibit programmed

Figure 9 Templated synthesis of polymer nanohelices via CVD polymerization into a nematic LC film. (A) Schematic representation of nanohelices 2S and 2R templated into the nematic E7 phase. Inset: Chemical representation of CVD polymerization of chiral and achiral precursors. (B–D) SEM images of nanohelices 2S and 2R and achiral nanofibers 2A prepared by CVD polymerization of 1S (B), 1R (C), and 1A (D), respectively (the LC is homeotropically anchored on a surface before polymerization and was removed prior to SEM). (E) High-resolution C1s XPS spectra of 2S and 2R confirming identical chemical composition for nanohelices with opposite handedness. (F) CD spectra of nanohelices 2S (blue) and 2R (green) and achiral nanofibers 2A (black). Adapted with permission from Ref. 87. Copyright 2022 John Wiley and Sons.

Figure 10 Changes in the optical appearance of an NFF-embedding LC under a) 0 V, b) 2.5 V, c) 10 V, and d) 0 V at 1 kHz (sine waveform, thickness ≈ 100 µm). Proposed mechanisms of side view (bottom) and top view (top) of nanofiber reorganization corresponding to each micrograph are described on the right-hand side. (e, f) A schematic illustration of the deformation of a single nanofiber on various planes. (g) The optical appearance of an NFF-embedding LC (10 V) with crossed polarizers and a wave plate (λ = 530 nm). The direction of the polarizer, the analyzer and the waveplate is indicated with the arrows. (h) Change in the average retardance of LC (a–c) as a function of voltage. The error bars are 1 S.D. of retardance measured across the sample (a–c, n = 92 points each). Adapted with permission from Ref. 90. Copyright 2022 John Wiley and Sons.

response under electric application, thereby stretching in *z*-direction by the elastic strain from the LC template (Figure 10). In this report, they used 65 mol% 4-(*trans*-4-pentylcyclohexyl) benzonitrile (PCH5) and 35 mol% 4-(*trans*-4-propylcyclohexyl) benzonitrile (PCH3) to induce bent anchoring at the LC–air interface and homeotropic anchoring at the indium tin oxide (ITO) glass substrate.[91]

Optical appearance under crossed polars showed dark brushes before the CVD polymerization, which comes from the extinct signals from the nanofibers that are parallel to either the analyzer or the polarizer orientation. Then PCP-HM was polymerized using CVD to synthesize bent nanofibers within the PCH mixture. Instead of removing the LC template, they placed another ITO substrate on top to prepare a sandwich cell. They applied an alternating current (AC) electric field (1 kHz) across the sandwich cell while observing under the cross-polarized microscope to characterize the changes in tilt angle of the LC–nanofiber composite. As shown in Figure 10a–d, optical retardance gradually decreased from 178 ± 22 nm to 5 ± 1 nm (Figure 10h), which indicates that mechanically coupled PCH/nanofibers were stretched by the elastic torque of the surrounding LC template during the electric field application. After removal of the AC, optical retardance increased again reversibly. To pro-

vide direct evidence of nanofiber actuation, they infused polymerizable LC (RM 257) and initiator to the PCH/nanofiber composite specimens. For comparison, they cross-linked the composite without an electric field and during the presence of an electric field. Then, both specimens were vitrified in liquid nitrogen to observe a cross-sectional view under cryogenic SEM. After coating the surface with Au/Pd in a vacuum environment, SEM images revealed that the tilt angle of nanofibers from the surface normal notably decreased under the presence of an electric field. Finally, a model was developed that predicts the equilibrium tilt angle of nanofibers under certain voltage of AC electric field. Their model predicted that the tilt angle changes from the initial angle of 60° to 27° upon 50 V of AC and this result was in good consistency with our observation under cryo-SEM. This report demonstrates a new type of system with shape-encoded actuation of end-attached nanofibers that resemble the behavior of a coral reef when capturing the preys into the core. Furthermore, mechanical modeling discussed in this report for the first time provides a quantitative assessment tool to evaluate the effect of elastic strain of LC matrix on the shape of end-attached nanofibers.

8 Conclusions and Outlook

This report provides a summary of significant research on CVD polymerization, which enables conformal deposition of polymer layers on a desired substrate. Functionalized PPXs can serve as reactive coatings and will facilitate the design of micro- and nano-structured biointerfaces. In addition, an overview of CVD of PCPs that can be performed on surfaces coated with thin films of LC to produce organized assemblies of end-attached polymer nanofibers is presented. The LC-templated CVD process is compatible with cholesteric LCs or blue-phase LC templates, allowing for the synthesis of a variety of nanofiber shapes. By virtue of the elastic energy stored in stretched nanofibers, these various nanofiber shapes offer the potential to program distinct electromechanical and electrooptical responses in LC–nanofiber composites. These results are encouraging for the development of advanced light valves and optical tweezers based on vortex light beams. The process resulted in the fabrication of soft nanocomposite materials encoding complex properties, such as responses to external fields that are promising for the design of new classes of electrooptical devices or soft actuators. The CVD polymerization of chiral precursors into LCs also results in superhierarchical arrangements of enantiomorphically pure nanofibers. Other LC phases exhibit distinct molecular orderings, and crystalline MOF networks with variable pores, crystal sizes, and shapes can serve as confined templates for the synthesis of three-dimensional polymer nanostructures.

The vapor deposition of PPX is a unique technique with numerous benefits that produces a polymer coating with exceptional properties. In 2022, the global PPX coating market was split by end-user industry (military and aerospace, electronics, medical, automotive), type (PPX-N, PPX-C, PPX-D), and geography (Asia-Pacific, North America, Europe, South America, and Middle-East and Africa).[92] The PPX coating market is anticipated to increase at a 5.8 % compound annual growth rate from 882.0 US\$ in 2022 to 1532.75 US\$ in 2030.[92] These projections show a significant increase in demand for PPX polymers in the future, highlighting the importance of this material across numerous industries. The conformal, functional, and responsive nature of CVD polymers makes them highly desirable in surface-modification applications. It was these materials' electronic and military uses that initially sparked scientific and industry attention. Having finally settled into a routine, the PPX polymers found new uses at the close of the 20th century, the most prevalent of which being MEMS (micro-electro-mechanical systems) technology. Due to MEMS, organic semiconductor, and biomedical applications, PPX has recently undergone a rebirth and appears to have extremely promising future prospects. However, there are disadvantages, such as the difficulties in synthesis of novel precursors, their high costs, and the sublimation of cyclophanes, which prevented a high throughput. Thus, research was conducted into employing different molecules as a beginning material. These chemicals must be volatile, thermodynamically stable, and capable of forming the required quinodimethane moiety. To obtain quantifiable PPX yields, quinodimethane moieties must be quantitatively generated from the starting material. All of these limits are unquestionably impediments to the growth of PPX, but their elimination will further establish the procedure as a real cross-sectional technology. Future studies may focus on CVD deposition kinetics under nano-confinement, ultra-high-aspect-ratio structures, and/or innovative templates. All of these factors play an ever-increasing significance in the creation of cutting-edge biomaterials. Additionally, the thickness of a polymer coating critically influences its mechanical properties. This mostly unexplored aspect has the potential to provide an additional control mechanism for fine-tuning local interactions.

Funding Information

Conflict of Interest

The authors declare no conflict of interest.

References

(1) Ramanathan, M.; Darling, S. B. *Prog. Polym. Sci.* **2011**, *36*, 793.

(2) Khlyustova, A.; Cheng, Y.; Yang, R. *J. Mater. Chem. B* **2020**, *8*, 6588.

(3) Lau, W.; Ismail, A.; Misdan, N.; Kassim, M. *Desalination* **2012**, *287*, 190.

(4) (a) Hammond, P. T. *AIChE J.* **2011**, *57*, 2928. (b) Wood, K. C.; Boedicker, J. Q.; Lynn, D. M.; Hammond, P. T. *Langmuir* **2005**, *21*, 1603. (c) Hammond, P. T. *Mater. Today* **2012**, *15*, 196. (d) Price, A. D.; Johnston, A. P. R.; Such, G. K.; Caruso, F. *Reaction Vessels Assembled by the Sequential Adsorption of Polymers* In Caruso, F., Ed., *Modern Techniques for Nano- and Microreactors/-reactions. Advances in Polymer Science, Vol. 229*; Springer: Berlin, **2010**, p. 115.

(5) Xue, F.; Liu, Z.; Su, Y.; Varahramyan, K. *Microelectron. Eng.* **2006**, *83*, 298.

(6) (a) Sukanek, P. C. *J. Imaging Technol.* **1985**, *11*, 184. (b) Yimsiri, P.; Mackley, M. R. *Chem. Eng. Sci.* **2006**, *61*, 3496. (c) Li, X.; Prukop, S. L.; Biswal, S. L.; Verduzco, R. *Macromolecules* **2012**, *45*, 7118. (d) Ma, C.; Zhou, H.; Wu, B.; Zhang, G. *ACS Appl. Mater. Interfaces* **2011**, *3*, 455.

(7) Lau, K. K.; Gleason, K. K. *Macromolecules* **2006**, *39*, 3688.

(8) (a) Rodger, D. C.; Fong, A. J.; Li, W.; Ameri, H.; Ahuja, A. K.; Gutierrez, C.; Lavrov, I.; Zhong, H.; Menon, P. R.; Meng, E. *Sens. Actuators, B* **2008**, *132*, 449. (b) Chen, H.-Y.; Lahann, J. *Langmuir* **2011**, *27*, 34.

(9) Dion, C. D.; Tavares, J. R. *Powder Technol.* **2013**, *239*, 484.

(10) Choy, K. *Prog. Mater. Sci.* **2003**, *48*, 57.

(11) Rajabi, H.; Mosleh, M. H.; Mandal, P.; Lea-Langton, A.; Sedighi, M. *Sci. Total Environ.* **2020**, *727*, 138654.

(12) Winterton, N. *Clean Technol. Environ. Policy* **2021**, *23*, 2499.

(13) Marvaniya, H. M.; Modi, K. N.; Sen, D. J. *Int. J. Drug Dev. Res.* **2011**, *3*, 42.

(14) Saini, R. D. *Int. J. Oceans Oceanogr.* **2017**, *11*, 217.

(15) Varma, R. S. *ACS Sustainable Chem. Eng.* **2016**, *4*, 5866.

(16) Yagüe, J. L.; Coclite, A. M.; Petruczok, C.; Gleason, K. K. *Macromol. Chem. Phys.* **2013**, *214*, 302.

(17) Alf, M. E.; Asatekin, A.; Barr, M. C.; Baxamusa, S. H.; Chelawat, H.; Ozaydin-Ince, G.; Petruczok, C. D.; Sreenivasan, R.; Tenhaeff, W. E.; Trujillo, N. J. *Adv. Mater.* **2010**, *22*, 1993.

(18) Pierson, H. O. *Handbook of Chemical Vapor Deposition-Principles, Technology and Application*; William Andrew Publishing: New York, **1999**, p. 36.

(19) Choy, K. L. *Chemical Vapour Deposition (CVD). Advances, Technology and Applications*; CRC Press: Boca Raton, **2019**, p. 71.

(20) Martin, T. P.; Lau, K. K.; Chan, K.; Mao, Y.; Gupta, M.; O'Shaughnessy, W. S.; Gleason, K. K. *Surf. Coat. Technol.* **2007**, *201*, 9400.

(21) d'Agostino, R.; Cramarossa, F.; Illuzzi, F. *J. Appl. Phys.* **1987**, *61*, 2754.

(22) Fan, Z.; Engel, J.M.; Chen, J.; Liu, C. *IEEE,* **2004**, *13*, 486.

(23) (a) Tenhaeff, W. E.; Gleason, K. K. *Adv. Funct. Mater.* **2008**, *18*, 979. (b) Winther-Jensen, B.; West, K. *Macromolecules* **2004**, *37*, 4538.

(24) Moss, T.; Greiner, A. *Adv. Mater. Interfaces* **2020**, *7*, 1901858.

(25) Gorham, W. F. *J. Polym. Sci., Part A: Polym. Chem.* **1966**, *4*, 3027.

(26) Szwarc, M. *Discuss. Faraday Soc.* **1947**, *2*, 46.

(27) Rogojevic, S.; Moore, J. A.; Gill, W. N. *J. Vac. Sci. Technol., A* **1999**, *17*, 266.

(28) Lahann, J. *Polym. Int.* **2006**, *55*, 1361.

(29) Wu, M.-G.; Hsu, H.-L.; Hsiao, K.-W.; Hsieh, C.-C.; Chen, H.-Y. *Langmuir* **2012**, *28*, 14313.

(30) Lahann, J.; Klee, D.; Pluester, W.; Hoecker, H. *Biomaterials* **2001**, *22*, 817.

(31) Xie, F.; Deng, X.; Kratzer, D.; Cheng, K. C. K.; Friedmann, C.; Qi, S.; Solorio, L.; Lahann, J. *Angew. Chem. Int. Ed.* **2017**, *56*, 203.

(32) Hopf, H. *Angew. Chem. Int. Ed.* **2008**, *47*, 9808.

(33) Bier, A. K.; Bognitzki, M.; Schmidt, A.; Greiner, A.; Gallo, E.; Klack, P.; Schartel, B. *Macromolecules* **2012**, *45*, 633.

(34) Elkasabi, Y.; Chen, H.-Y.; Lahann, J. *Adv. Mater.* **2006**, *18*, 1521.

(35) Lahann, J. *Chem. Eng. Commun.* **2006**, *193*, 1457.

(36) Chen, Y.-C.; Sun, T.-P.; Su, C.-T.; Wu, J.-T.; Lin, C.-Y.; Yu, J.; Huang, C.-W.; Chen, C.-J.; Chen, H.-Y. *ACS Appl. Mater. Interfaces* **2014**, *6*, 21906.

(37) Elkasabi, Y.; Lahann, J. *Macromol. Rapid Commun.* **2009**, *30*, 57.

(38) Wood, R. *Mater. World* **2000**, *8*, 30.

(39) Yu, Q.; Deffeyes, J.; Yasuda, H. *Prog. Org. Coat.* **2001**, *41*, 247.

(40) Hanefeld, P.; Sittner, F.; Ensinger, W.; Greiner, A. *e-Polymers* **2006**, *26,* 1.

(41) Lahann, J.; Choi, I. S.; Lee, J.; Jensen, K. F.; Langer, R. *Angew. Chem. Int. Ed.* **2001**, *40*, 3166.

(42) Klee, D.; Weiss, N.; Lahann, J. *Vapor-Based Polymerization of Functionalized [2.2]Paracyclophanes: A Unique Approach towards Surface-Engineered Microenvironments* In Gleiter, R.; Hopf, H., Eds., *Modern Cyclophane Chemistry, Chap. 18*; Wiley-VCH: Weinheim, **2004**, p. 463.

(43) Lahann, J.; Klee, D.; Höcker, H. *Mater. Sci. Eng.* **1999**, *30*, 763.

(44) Bates. B.; Ragheb. A.; Fearnot. N.; Voorhees. W.; Kozma. T.; Grewe. D.; Schaeffer. D. *U. S. Pat. Appl. Publ.* **1997**, *8,* 484.

(45) (a) Weisenberg, B. A.; Mooradian, D. L. *J. Biomed. Mater. Res.* **2002**, *60*, 283. (b) Ryu, K. S.; Shaikh, K.; Goluch, E.; Fan, Z.; Liu, C. *Lab Chip* **2004**, *4*, 608.

(46) (a) Alrifaiy, A.; Lindahl, O. A.; Ramser, K. *Polymers.* **2012**, *4*, 1349. (b) Teles, F. R. R.; Fonseca, L. P. *Mater. Sci. Eng., C* **2008**, *28*, 1530.

(47) Nandivada, H.; Chen, H. Y.; Lahann, J. *Macromol. Rapid Commun.* **2005**, *26*, 1794.

(48) Kashima, Y.; Munakata, T.; Matoba, A. *Opt. Rev.* **1997**, *4*, A69.

(49) Lahann, J.; Langer, R. *Macromolecules* **2002**, *35*, 4380.

(50) (a) Lahann, J.; Balcells, M.; Lu, H.; Rodon, T.; Jensen, K. F.; Langer, R. *Anal. Chem.* **2003**, *75*, 2117. (b) Jiang, X.; Chen, H. Y.; Galvan, G.; Yoshida, M.; Lahann, J. *Adv. Funct. Mater.* **2008**, *18*, 27.

(51) Deng, X.; He, S.; Xie, F.; Friedmann, C.; Hess, H.; Lahann, J. *Adv. Mater.* **2016**, *28*, 2367.

(52) Xia, Y. N.; Whitesides, G. M. *Annu. Rev. Mater. Sci.* **1998**, *28*, 153.

(53) Kumar, A.; Whitesides, G. M. *Appl. Phys. Lett.* **1993**, *63*, 2002.

(54) Chen, H.-Y.; Lahann, J. *Anal. Chem.* **2005**, *77*, 6909.

(55) Suh, K. Y.; Langer, R.; Lahann, J. *Appl. Phys. Lett.* **2003**, *83*, 4250.

(56) Chen, H.-Y.; Hirtz, M.; Deng, X.; Laue, T.; Fuchs, H.; Lahann, J. *J. Am. Chem. Soc.* **2010**, *132*, 18023.

(57) Im, S. G.; Kim, B.-S.; Lee, L. H.; Tenhaeff, W. E.; Hammond, P. T.; Gleason, K. K. *Macromol. Rapid Commun.* **2008**, *29*, 1648.

(58) (a) Wang, M.; Wang, X.; Moni, P.; Liu, A.; Kim, D. H.; Jo, W. J.; Sojoudi, H.; Gleason, K. K. *Adv. Mater.* **2017**, *29*, 1604606. (b) Yu, S. J.; Pak, K.; Kwak, M. J.; Joo, M.; Kim, B. J.; Oh, M. S.; Baek, J.; Park, H.; Choi, G.; Kim, D. H.; Choi, J.; Choi, Y.; Shin, J.; Moon, H.; Lee, E.; Im, S. G. *Adv. Eng. Mater.* **2018**, *20*, 1700622.

111

Organic Materials   T. Mohammadi Hafshejani et al.   THIEME OPEN ACCESS   **Short Review**

(59) (a) Kim, J.; Jang, S. C.; Bae, K.; Park, J.; Kim, H.-D.; Lahann, J.; Kim, H.-S.; Lee, K. J. *ACS Appl. Mater. Interfaces* **2021**, *13*, 43123. (b) Deng, X.; Lahann, J. *J. Appl. Polym. Sci.* **2014**, *131*, 40315.

(60) Parsons, G. N. *J. Vac. Sci. Technol., A* **2019**, 37, 020911.

(61) Parsons, G. N.; Clark, R. D. *Chem. Mater.* **2020**, *32*, 4920.

(62) Gladfelter, W. L. *Chem. Mater.* **1993**, *5*, 1372.

(63) Vaeth, K. M.; Jensen, K. F. *Adv. Mater.* **1999**, *11*, 814.

(64) Vaeth, K. M.; Jensen, K. F. *Chem. Mater.* **2000**, *12*, 1305.

(65) Chen, H.-Y.; Lai, J. H.; Jiang, X.; Lahann, J. *Adv. Mater.* **2008**, *20*, 3474.

(66) Vitos, L.; Ruban, A.; Skriver, H. L.; Kollár, J. *Surf. Sci.* **1998**, *411*, 186.

(67) Yu, N. F.; Tian, N.; Zhou, Z. Y.; Huang, L.; Xiao, J.; Wen, Y. H.; Sun, S. G. *Angew. Chem. Int. Ed.* **2014**, *53*, 5097.

(68) Xiao, C.; Lu, B.-A.; Xue, P.; Tian, N.; Zhou, Z.-Y.; Lin, X.; Lin, W.-F.; Sun, S.-G. *Joule* **2020**, *4*, 2562.

(69) Fortin, J. B.; Lu, T. M. *Chem. Mater.* **2002**, *14*, 1945.

(70) Lee, I. J.; Yun, M. *Macromolecules* **2010**, *43*, 5450.

(71) (a) Kolahalam, L. A.; Kasi Viswanath, I. V.; Diwakar, B. S.; Govindh, B.; Reddy, V.; Murthy, Y. L. N. *Mater. Today Proc.* **2019**, *18*, 2182. (b) Abid, N.; Khan, A. M.; Shujait, S.; Chaudhary, K.; Ikram, M.; Imran, M.; Haider, J.; Khan, M.; Khan, Q.; Maqbool, M. *Adv. Colloid Interface Sci.* **2021**, *300*, 102597.

(72) Tung, H.-Y.; Guan, Z.-Y.; Liu, T.-Y.; Chen, H.-Y. *Nat. Commun.* **2018**, *9*, 4383.

(73) Wu, C.-Y.; Wu, T.-Y.; Guan, Z.-Y.; Wang, P.-Y.; Yang, Y.-C.; Huang, C.-W.; Lin, T.-H.; Chen, H.-Y. *Nat. Commun.* **2021**, *12*, 3413.

(74) Begum, S.; Behboodi-Sadabad, F.; Pramudya, Y.; Dolle, C.; Kozlowska, M.; Hassan, Z.; Mattern, C.; Gorji, S.; Heißler, S.; Welle, A. *Chem. Mater.* **2022**, *34*, 6268.

(75) (a) Majdecki, M.; Niedbala, P.; Jurczak, J. *ChemistrySelect* **2020**, *5*, 6424. (b) Majdecki, M.; Tyszka-Gumkowska, A.; Jurczak, J. *Org. Lett.* **2020**, *22*, 8687. (c) Majdecki, M.; Grodek, P.; Jurczak, J. *J. Org. Chem.* **2021**, *86*, 995.

(76) Gonay, M.; Batisse, C.; Paquin, J.-F. *Synthesis* **2020**, *53*, 653.

(77) Nairoukh, Z.; Strieth-Kalthoff, F.; Bergander, K.; Glorius, F. *Chem. Eur. J.* **2020**, *26*, 6141.

(78) Slivka, M.; Onysko, M. *Synthesis* **2021**, *53*, 3497.

(79) Zeng, J.; Aigner, A.; Czubayko, F.; Kissel, T.; Wendorff, J. H.; Greiner, A. *Biomacromolecules* **2005**, *6*, 1484.

(80) Demirel, M. C. *Colloids Surf., A* **2008**, *321*, 121.

(81) Noorduin, W. L.; Grinthal, A.; Mahadevan, L.; Aizenberg, J. *Science* **2013**, *340*, 832.

(82) Williams, A. H.; Roh, S.; Jacob, A. R.; Stoyanov, S. D.; Hsiao, L.; Velev, O. D. *Nat. Commun.* **2021**, *12*, 2834.

(83) (a) Tsuei, M.; Tran, H.; Roh, S.; Ober, C. K.; Abbott, N. L. *Macromolecules* **2021**, *54*, 7786. (b) Poulin, P.; Raghunathan, V.; Richetti, P.; Roux, D. *Science* **1994**, *275*, 1770.

(84) Mitani, M.; Ogata, S.; Yamane, S.; Yoshio, M.; Hasegawa, M.; Kato, T. *J. Mater. Chem. C* **2016**, *4*, 2752.

(85) Akagi, K.; Piao, G.; Kaneko, S.; Sakamaki, K.; Shirakawa, H.; Kyotani, M. *Science* **1998**, *282*, 1683.

(86) Cheng, K. C.; Bedolla-Pantoja, M. A.; Kim, Y.-K.; Gregory, J. V.; Xie, F.; De France, A.; Hussal, C.; Sun, K.; Abbott, N. L.; Lahann, J. *Science* **2018**, *362*, 804.

(87) Varadharajan, D.; Nayani, K.; Zippel, C.; Spuling, E.; Cheng, K. C.; Sarangarajan, S.; Roh, S.; Kim, J.; Trouillet, V.; Bräse, S. *Adv. Mater.* **2022**, *34*, 2108386.

(88) Yang, J.; Li, P.; Zhao, B.; Pan, K.; Deng, J. *Nanoscale Adv.* **2020**, *2*, 1301.

(89) Zhao, B.; Yu, H.; Pan, K.; Tan, Z. a.; Deng, J. *ACS Nano* **2020**, *14*, 3208.

(90) Roh, S.; Kim, J.; Varadharajan, D.; Lahann, J.; Abbott, N. L. *Adv. Funct. Mater.* **2022**, *32*, 2200830.

(91) Nayani, K.; Rai, P.; Bao, N.; Yu, H.; Mavrikakis, M.; Twieg, R. J.; Abbott, N. L. *Adv. Mater.* **2018**, *30*, 1706707.

(92) GlobeNewswire; https://www.globenewswire.com/en/news-release/2022/09/12/2514100/0/en/Conformal-Coatings-Market-is-estimated-to-be-US-1532-75-million-by-2030-with-a-CAGR-of-5-8-during-the-forcast-period-By-PML.html (accessed September 12, 2022).